Groundwater

Calibrating a Salt Water Intrusion Model with Time-Domain Electromagnetic Data

by Daan Herckenrath[1], Nick Odlum[2], Vanessa Nenna[2], Rosemary Knight[2], Esben Auken[3], and Peter Bauer-Gottwein[4]

Abstract

Salt water intrusion models are commonly used to support groundwater resource management in coastal aquifers. Concentration data used for model calibration are often sparse and limited in spatial extent. With airborne and ground-based electromagnetic surveys, electrical resistivity models can be obtained to provide high-resolution three-dimensional models of subsurface resistivity variations that can be related to geology and salt concentrations on a regional scale. Several previous studies have calibrated salt water intrusion models with geophysical data, but are typically limited to the use of the inverted electrical resistivity models without considering the measured geophysical data directly. This induces a number of errors related to inconsistent scales between the geophysical and hydrologic models and the applied regularization constraints in the geophysical inversion. To overcome these errors, we perform a coupled hydrogeophysical inversion (CHI) in which we use a salt water intrusion model to interpret the geophysical data and guide the geophysical inversion. We refer to this methodology as a Coupled Hydrogeophysical Inversion-State (CHI-S), in which simulated salt concentrations are transformed to an electrical resistivity model, after which a geophysical forward response is calculated and compared with the measured geophysical data. This approach was applied for a field site in Santa Cruz County, California, where a time-domain electromagnetic (TDEM) dataset was collected. For this location, a simple two-dimensional cross-sectional salt water intrusion model was developed, for which we estimated five uniform aquifer properties, incorporating the porosity that was also part of the employed petrophysical relationship. In addition, one geophysical parameter was estimated. The six parameters could be resolved well by fitting more than 300 apparent resistivities that were comprised by the TDEM dataset. Except for three sounding locations, all the TDEM data could be fitted close to a root-mean-square error of 1. Possible explanations for the poor fit of these soundings are the assumption of spatial uniformity, fixed boundary conditions and the neglecting of 3D effects in the groundwater model and the TDEM forward responses.

Introduction

Salt water intrusion models are commonly used to quantify the impact of groundwater withdrawals and sea level rise on coastal fresh water resources (Zhang et al. 2004; Giambastiani et al. 2007; Lebbe et al. 2008). Complex geological structures and the limited amount of information about the current level of salt water intrusion are typical features complicating groundwater management. Previous studies have demonstrated the ability of electromagnetic (EM) data to determine the extent of salt water intrusion at many sites in the world (e.g., Fitterman and Stewart 1986; Goldman et al. 1991; Frohlich et al. 1994; Duque et al. 2008; Adepelumi

[1]Corresponding author: Department of Environmental Engineering, Technical University of Denmark, Miljøvej, Bldg. 113, DK-2800, Kgs. Lyngby, Denmark; daan.herckenrath@flinders.edu.au

[2]Department of Geophysics, Stanford University, Panama Mall 397, 8000 Stanford, CA.

[3]Department of Geoscience, Aarhus University, Høegh-Guldbergs Gade 2, 8000 Aarhus C, Denmark.

[4]Department of Environmental Engineering, Technical University of Denmark, Miljøvej, Bldg. 113, DK-2800, Kgs. Lyngby, Denmark.

Received December 2011, accepted June 2012.

doi: 10.1111/j.1745-6584.2012.00974.x

et al. 2009; Abdalla et al. 2010). EM methods have also been used to image hydrogeologic structure for use in conjunction with hydrologic models (Fitterman and Stewart 1986; Auken et al. 2006; Koukadaki et al. 2007). These datasets are very appealing to hydrogeologists because they provide a level of spatial sampling at a scale that cannot be obtained using more traditional borehole methods. Applications of airborne EM surveys in coastal aquifers include mapping of salt water intrusion in the United States (Langevin et al. 2003), buried valleys in Denmark (Auken et al. 2008), subsurface salt loads in Australia (Mullen et al. 2007), and a partially salt water-filled cave system in Mexico (Supper et al. 2009).

Similar in application to the work of Nenna et al. (unpublished data), this study is focused on the use of EM data to provide information of interest to water managers in coastal urban areas in Santa Cruz and Monterey Counties, California. In Nenna et al. (unpublished data), EM methods are evaluated to act as non-invasive alternatives to the use of sentinel wells to monitor salt water intrusion in coastal aquifer systems and to characterize the continuity of important confining units. In this study, we present a framework, based on Kowalsky et al. (2005), Lambot et al. (2009), Hinnell et al. (2010), and Pollock and Cirpka (2010), to integrate EM data into salt water intrusion models using a coupled hydrogeophysical inversion (CHI) approach.

Ferré et al. (2009) and Hinnell et al. (2010) provide an overview of different methods to incorporate geophysical data into hydrological models. In this study, we highlight two of these approaches, a sequential hydrogeophysical inversion (SHI) approach and the CHI approach. In an SHI, a geophysical inversion is performed after which a hydrologic model is calibrated using the estimated geophysical parameters as additional observations. When using an SHI, the geophysical inversion is performed independently and geophysical measurement errors and parameter resolution errors are propagated into the hydrological model (Hinnell et al. 2010). With a CHI, a hydrological model is embedded within the geophysical inversion process. In this approach, a hydrologic model is used to offer an interpretation framework for the geophysical data by simulating a hydrologic state variable (e.g., moisture content or solute concentration), which is subsequently translated into a geophysical parameter distribution using a petrophysical relationship (e.g., Archie 1942; Topp et al. 1980). The simulated geophysical forward responses (e.g., apparent resistivity and EM wave velocity) are subsequently compared with the geophysical observations. We refer to this methodology as a Coupled Hydrogeophysical Inversion-State (CHI-S).

The CHI-S has been successfully applied for reducing parameter uncertainty in hydrological models for estimating water content and solute concentrations using ground penetrating radar and electrical resistivity tomography data (Kowalsky et al. 2005; Lambot et al. 2009; Hinnell et al. 2010; Pollock and Cirpka 2010). In Bauer-Gottwein et al. (2009), the CHI-S approach is used for a variable-density groundwater flow model and time-domain electromagnetic (TDEM) data, but this study primarily focused on the limitation of standard one-dimensional (1D) TDEM forward models to interpret the three-dimensional (3D) nature of subsurface anomalies caused by salt transport phenomena.

The intention of this study is to demonstrate the potential of the CHI-S approach as a way to inform regional salt water intrusion models with TDEM data. In particular, we want to show the ability of a salt water intrusion model to offer a powerful physical interpretation framework for guiding the geophysical inversion process by comparing geophysical models, obtained using traditional geophysical inversion approaches, with the results of the CHI-S. Furthermore, parameter estimation results will be shown for a salt water intrusion model and results will be provided to illustrate how well TDEM observations can be fitted using the CHI-S. For this purpose, we first provide a description of the CHI-S approach, after which we give an overview of the field site for which we apply the CHI-S. Then a description is provided of the TDEM data and the salt water intrusion model that was used for demonstrating the CHI-S. We then discuss the advantages of applying the CHI-S with respect to the SHI approach.

Methodology

Sequential and Coupled Hydrogeophysical Inversion

The left panel of Figure 1 provides a visual description of a Sequential Hydrogeophysical Inversion-State (SHI-S) framework and its implementation for a salt water intrusion model. The SHI-S, which is investigated in previous studies (Langevin et al. 2003; Macaulay and Mullen 2007), consists of three steps, in which first a geophysical inversion is performed where geophysical parameter distributions (π) are estimated by minimizing a geophysical misfit function (Φ_g) that comprises differences between observed and simulated geophysical data and often a number of regularization constraints (e.g., smoothness constraints). The estimated geophysical parameters (e.g., electrical resistivities) can act as observations for the salt water intrusion model by applying a petrophysical relationship between the estimated geophysical parameters and the simulated salt concentrations. The final step is to perform a calibration in which the input parameters of the salt water intrusion model (γ) are estimated using the estimated geophysical parameters as observation data. The misfit function (Φ_{SHI}) that is minimized in the SHI-S comprises the difference between simulated and observed hydrological data (Φ_h) and simulated hydrological data versus the estimated geophysical parameter distributions (Φ_s).

The right panel of Figure 1 shows the CHI-S approach. In the CHI-S, three groups of parameters are estimated: hydrological parameters (γ), petrophysical parameters (p), and uncoupled geophysical parameters (π_u). First, a salt water intrusion model is calculated,

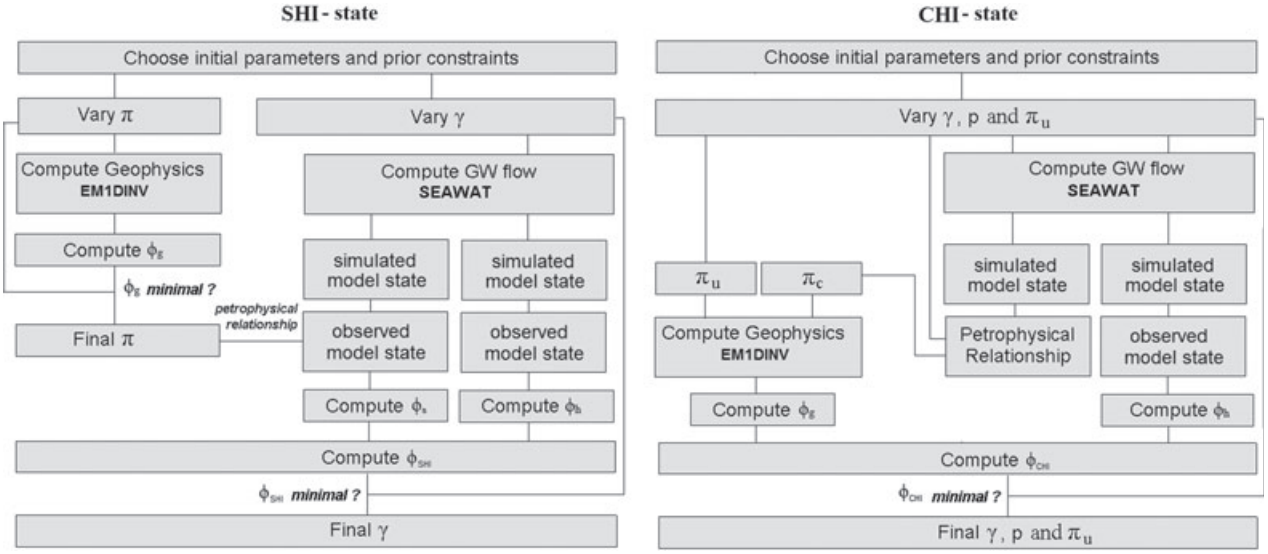

Figure 1. Inversion framework for a salt water intrusion model and TDEM data using a sequential (left) and coupled hydrogeophysical inversion approach (right).

after which the simulated salt concentrations are translated to geophysical parameters (π_c) using a petrophysical relationship. The employed petrophysical relationship can contain site-specific parameters that need to be estimated in the CHI-S as well. Finally, geophysical parameters in π_c might not be able to describe a complete geophysical parameter distribution (e.g., electrical resistivities of deep geological layers that extend beyond the range of the salt water intrusion model) in order to obtain a satisfactory fit to the geophysical data. For this reason, a number of geophysical parameters can be estimated directly in the CHI-S (π_u). Based on π_c and π_u, a complete geophysical parameter distribution can be derived in order to generate a geophysical forward response that can be compared with the geophysical measurement data. The misfit function (Φ_{CHI}) that is minimized in the CHI-S comprises the difference between simulated and observed hydrologic data (Φ_h) and simulated versus observed geophysical data (Φ_g).

Implementation

The CHI-S was implemented using the optimization software PEST (Doherty 2010), which employs the Levenberg-Marquardt gradient-search algorithm. The SEAWAT computer program (Langevin and Guo 2006) was used for simulating groundwater flow and salt concentrations. In this study, we use simulated salt concentrations to generate the parameter distributions for the TDEM model. For this purpose, we employ the Archie's law (Archie 1942) for a fully water-saturated system:

$$\rho = \rho_{gw}\varphi^{-m} \quad (1)$$

where m is a cementation factor, which typically ranges from 1.3 for unconsolidated sands to 2 for consolidated sandstones. As the Archie's law implicitly assumes that the total porosity is equal to the effective porosity of the medium (Lesmes and Friedman 2005), φ can be replaced by the saturated water content θ_s. θ_s^{-m} is equal to the formation factor F.

To generate TDEM forward responses, we used the EM1DINV software developed by the Aarhus University (HGG 2011). The forward modeling algorithm used in EM1DINV is based on Ward and Hohmann (1988) and includes the modeling of low-pass filters according to Effersø et al. (1999) and the turn-on and turn-off ramps described by Fitterman and Anderson (1987). The forward responses are generated for 1D electrical resistivity models. 3D approaches are available to generate a TDEM forward response (e.g., Newman et al. 1986; Wang and Hohmann 1993; Commer and Newman 2004; Bauer-Gottwein et al. 2009), but these often require an impractically large computational burden. Depending on the spatial scale on which salt water intrusion acts, these 3D effects might be relevant, but this problem is beyond the scope of this investigation.

Case Study: School Grounds

To demonstrate the CHI-S for salt water intrusion models, we developed a simple cross-sectional salt water intrusion model for a field site, which is on the grounds of a private school located within the Pajaro Valley, a coastal watershed of 400 km^2 adjacent to the Pacific Ocean in Santa Cruz County, California. We refer to this site as the School-site. At this location, 19 TDEM soundings were collected to inform the salt water intrusion model. A map of the School-site is given in Figure 2, showing its main properties and the location of the acquired TDEM soundings. In the following, we provide a short description of the hydrogeological setting of this location, the collected TDEM data, and the objective, setup, and simplifications associated with the salt water intrusion and TDEM models.

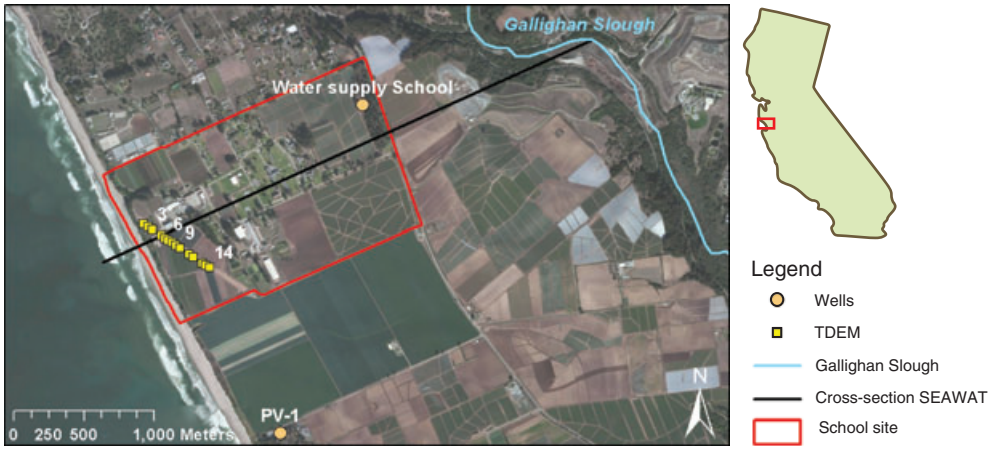

Figure 2. Aerial map of the School-site (left), providing an overview of the TDEM-sounding locations, boreholes, and the cross section for which the SEAWAT simulations are performed.

Hydrogeology and Groundwater Data

At the School-site, three major geological units can be distinguished that are relevant for groundwater flow. These geological units reside on top of relatively impermeable granite basement rock from the Cretaceous. From bottom to top, these three units are the Purisima Formation (poorly consolidated Miocene-Pliocene marine deposits), the Aromas Sand (unconsolidated Pleistocene deposits), and the shallow Alluvium (unconsolidated Holocene dune deposits). In addition, the Aromas Sand can be subdivided into an upper and lower portion on the basis of lithology and geophysical characteristics (Hanson 2003). The aquifer system of Pajaro Valley consists of three principal aquifers: a deep aquifer at ca. −90 mamsl comprised of the Lower Aromas Sand and Purisma Formation, a primary aquifer in the Upper Aromas Sands, and an unconfined aquifer within the same unit (Bond and Bredehoeft 1987; Hanson 2003). In this research, we will only focus on the unconfined aquifer, comprised of the Upper Aromas Sand deposits and the shallow Alluvium. The confining unit between the unconfined aquifer and the primary aquifer is a geologically complex layer, including alluvial clays, marine clays that extend onshore, indurated clays and iron-oxide cementation zones in dune and terrace deposits, paleosols, and fluvial clay lenses in the Aromas Sand (Bond and Bredehoeft 1987).

The Upper Aromas deposits are layered marine and terrestrial coarse-grained deposits separated by extensive fine-grained deposits that potentially restrict the vertical movement of groundwater and sea water intrusion. Lowered groundwater levels caused by overdraft in coastal areas have resulted in widespread sea water intrusion in the Aromas Sands, starting as early as 1947 (Mann 1988). As many of the wells in the coastal and inland subregions are screened at depths of 60 to 90 m below land surface, a direct avenue is provided for sea water intrusion through the coarse-grained deposits of the shallower alluvium and Aromas Sand. Geophysical logs from monitoring wells indicate not only discrete zones of saline water that are related to sea water intrusion in the aquifer of the shallow Alluvium and the Upper Aromas Sand, but also salt water intrusion in the deep aquifer system of the Lower Aromas Sand (Hanson 2003).

Near the School-site, one borehole description was available for the water supply well that is marked in Figure 2, showing a ca. 13-m thick sandy clay layer at an elevation of −40 mamsl. A gamma log at approximately 2 km from the site (borehole PV-1 in Hanson 2003) indicated sandy clay deposits with a thickness of ca. 5 m at an elevation of approximately −15 mamsl. These deposits likely mark the confining unit between the unconfined aquifer and the primary aquifer. No concentration and water level data were available for the School-site (Figure 3).

TDEM Data

At the School-site, 19 TDEM soundings were collected on an air strip to obtain a transect of TDEM soundings that can be used for a 2D resistivity model representing electrical resistivity variations perpendicular to the coast. We will refer to the individual soundings as TDEM 1, TDEM 2, etc., where the increasing sounding number represents soundings further away from the coast. TDEM soundings 15 to 19 did not yield data of satisfactory quality, which can be attributed to environmental noise. Such noise sources can include buried debris and cables, but at the School-site the noise was primarily attributed to the presence of metal irrigation pipes. TDEM data were collected using a Geonics ProTEM 47 (Geonics Limited, Mississauga, Ontario, Canada). For the measurements, a 20-m double-turn transmitter loop was used due to the limited width of the air strip. Data were collected at ultra-high and very-high frequencies employing 20 time gates for each frequency mode. Both offset and center-loop receiver configurations were used, but, in this research, we only use the center-loop data as the offset receiver geometry produced noisier data.

To process the TDEM data, we used the SiTEM software (HGG 2011), and then performed an initial inversion of the TDEM data using two different methods.

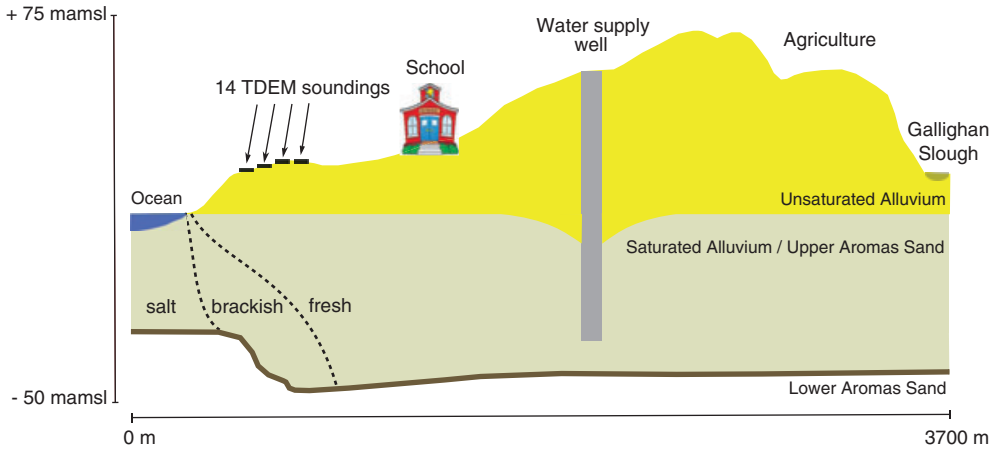

Figure 3. Hydrogeological schematic of the School-site.

An overview of different approaches for the inversion and modeling of TDEM data can be found in Oldenburg (1990). We applied a few-layer inversion in which a small number of layer thicknesses and layer conductivities were estimated for each sounding location without any regularization constraints. The second inversion method comprised a 25-layer smooth inversion using the EM1DTM code, in which layer thicknesses are fixed prior to inversion, and EM1DTM estimates the electrical resistivity of each layer by minimizing both the data misfit and a number of smoothness constraints (Farquharson and Oldenburg 1993). Data error varied between 3% and 5% to take into account errors that result from neglecting 3D effects and imperfect instrument specifications (e.g., filters and wave form of the applied pulses) in generating the TDEM forward responses in addition to the standard deviations of measured field data.

Figure 4A presents the inverted three-layer resistivity models for TDEM soundings 1 to 14 as a function of the distance from the coast. All electrical resistivity models show a first layer with a high resistivity, a second layer with a very low electrical resistivity, and a third layer with a higher resistivity compared with the second layer.

At the site, an unsaturated zone is present of approximately 20 m thickness, consisting of dry sandy deposits, which typically have an electrical resistivity of more than 100 Ωm (Kirsch 2006). Groundwater levels are expected to be close to ocean level. As the bottom of the first layer in Figure 4A occurs around −10 mamsl, this first layer can be interpreted as a layer comprising both the dry deposits and the fresh water-saturated aquifer. Furthermore, we can distinguish a second layer with a very low electrical resistivity of <1 Ωm. Given the setting within a coastal aquifer, this layer was interpreted as salt water-saturated sediments. The final third layer in Figure 4A is notable as it shows an increased electrical resistivity compared with the layer above. As fresh water is less dense compared with salt water, this third TDEM layer must represent a geological unit with different hydrogeologic properties that prevents the salt water from going down into the deeper aquifer system. The electrical resistivity values, which vary between 5 and 10 Ωm, indicate that this third layer likely represents a fresh water-saturated clay deposit. Note that the three-layer electrical resistivity model in Figure 4A assumes an infinite extension of the third layer, so no thickness can be derived for this clay deposit. In Figure 4A, we assigned an arbitrary thickness of 2 m to this layer for visualization purposes.

In the geophysical inversion, the electrical resistivity of the deepest TDEM layer cannot be well resolved due to the overlying layer of sea water, which is a very good electrical conductor that shields the layers underneath from induced eddy currents. Moreover, this layer may be highly heterogeneous in terms of thickness and elevation (as shown by PV-1 and the borehole report of the water supply well) and the salinity of the pore water. As Nenna et al. (unpublished data) show, the detection of this confining layer with TDEM is very important for risk assessment with regards to salt water intrusion in coastal aquifers adjacent to Monterey Bay. In Figure 4A, a dip can be seen associated with the clay layer. As the TDEM soundings are neither oriented perpendicular nor parallel to the coast, we do not know in which direction the dip is most significant. Based on the gamma log in PV-1 and the dipping rate of the Lower Aromas Sand documented in Hanson (2003), the dip in Figure 4A is likely to be oriented perpendicular to the coast. In this research, we will only consider the unconfined aquifer and use the elevation of the third TDEM layer to represent the bottom boundary of this aquifer. Figure 4B is the inversion result for the 25-layer smooth model that shows a similar sequence of electrical resistivities of, respectively, high, low, and high values that could be observed in Figure 4A. Figure 4C will be discussed at a later stage, as it encompasses the result of the CHI-S.

Salt Water Intrusion Model

The main purpose for the investigations at the School-site is to evaluate whether we can successfully retrieve the hydrogeologic properties of this site using the TDEM

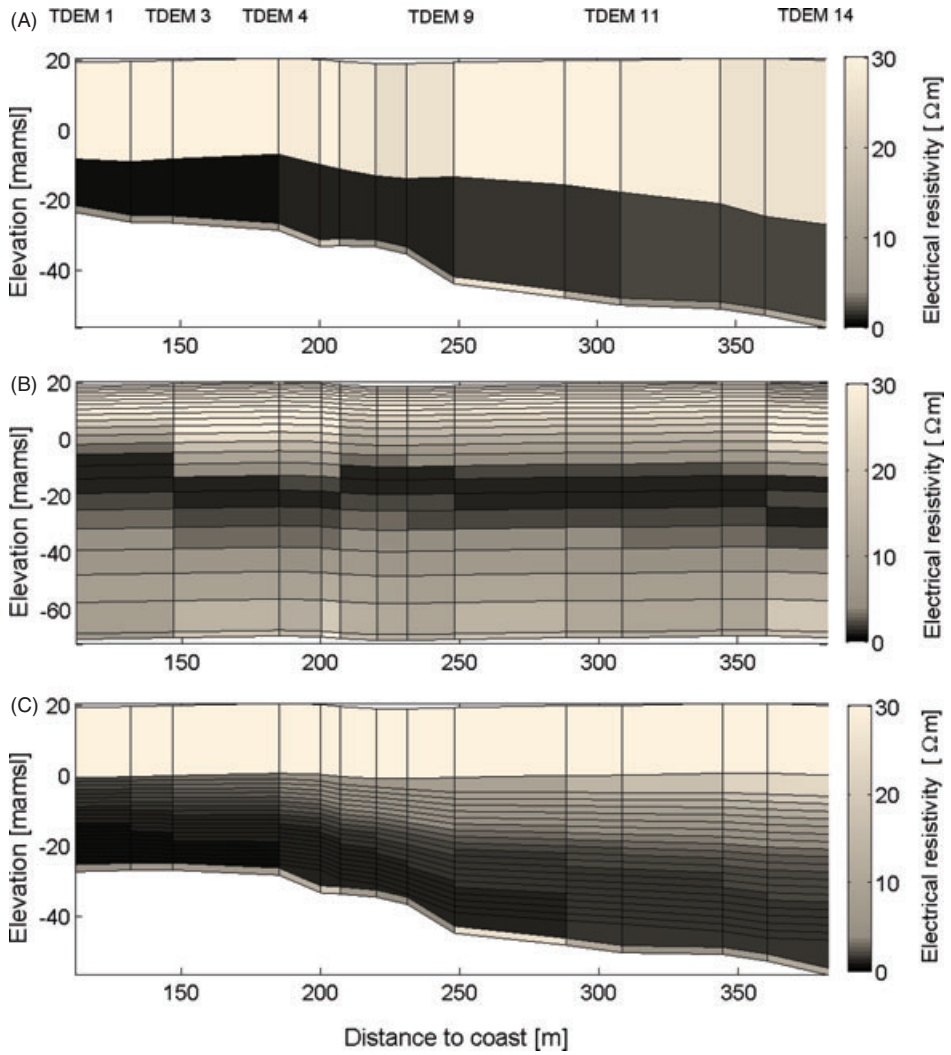

Figure 4. Inversion results of the 14 TDEM soundings using (A) a three-layer electrical resistivity model, (B) 25-layer smooth inversion, and (C) CHI-S inversion.

data only. For the School-site, we developed a vertical 2D cross-sectional salt water intrusion model to simulate salt water intrusion due to the pumping activities near the Monterey Bay Academy and obtain a range of values for the key hydrogeologic properties of the Upper Aromas Sand at this location.

The model has a length of ca. 3700 m and a depth of ca. 40 to 60 m. The assumption of a cross-sectional model implies neglecting groundwater flow parallel to the coast and the influences that are caused by groundwater pumping at locations close to the School-site. The land use around the School-site is predominantly agricultural (Hanson 2003), using groundwater for crop irrigation. For the salt water intrusion model, we use the ocean as a west boundary for which we assume hydrostatic sea water conditions with a constant concentration C_s of 35 kg/m^3 and a hydraulic head of 0 mamsl. To control the water flux at the east boundary, we apply a drain condition that represents a draining channel named Gallighan Slough. The drainage level of this channel was set to +3 mamsl, which corresponds to its bottom elevation. The drain conductivity was assumed to be equal to the hydraulic conductivity of the unconfined aquifer, the value of which will be discussed in the next paragraph. The groundwater recharge rate applied on top of the model was equal to 0.35 ft/year, which corresponds to 107 mm/year. This value was based on earlier investigations by CH2M/HILL (2005). No-flow conditions are specified for the bottom of the model. Bond and Bredehoeft (1987) indicated a marginal flow from the unconfined aquifer toward the deeper aquifer system but this process was disregarded in this research. The elevation of the bottom of the model was derived based on the inversion results of the TDEM soundings and one borehole at the School-site. The aquifer properties are represented by a uniform hydraulic conductivity, anisotropy, porosity, specific yield, dispersivity, and diffusion value. These will be estimated in the CHI-S; we elaborate on the estimation process in the next section.

For this study, we did not possess much information about the exact pumping history at and near the

Table 1
Variables and Input Parameters for the SEAWAT Simulations

Input Variables		Numerical Solution Parameters	
Recharge (mm/year)	107	Number columns	500
Extraction rate school (m^3/d)	950	Number layers	25
ρ_s (kg/m^3)	1025	Column size, dx (m)	7
ρ_f (kg/m^3)	1000	Layer size, dz (m)	ca. 1 to 2
C_s (kg/m^3)	35	Solver flow	PCG
m (−)	1.3	Head stop criterion (m)	10^{-2}
Estimated Parameters and Starting Values		Flow stop criterion (m^3/d)	10^{-2}
K_h (m/d)	20	Solver advective transport	Finite difference
K_z/K_h (−)	0.1	Concentration stop criterion (kg/m^3)	10^{-4}
S_y (−)	0.285	Solver dispersion and source terms	Implicit finite difference
α_L, α_T/α_L(−)	10, 0.1	Time step length (d)	20
D_m (m^{-2}/d)	10^{-4}		
θ_s, θ_{res}(−)	0.33, 0.045		

School-site. For the SEAWAT model, we assume one single water supply well positioned 1900 m from the coast, which corresponds approximately to one of the water supply wells at the School-site. Bond and Bredehoeft (1987) show a pumping rate between 7 and 28 L/s at this location. Recent daily extraction rates at the School-site amount to ca. 5 to 6 L/s. However, using a cross-sectional model implies that the applied pumping rate is uniformly distributed along the coastline (line sink). The extraction rate should therefore not be seen as the exact pumping rate for the supply wells at the School-site, but as the average value of groundwater extraction per unit length of the coast. Note our model extends further inland than the School-site only. Furthermore, many other pumping wells are present around the School-site (Hanson 2003); the influence of these wells is not directly taken into account using the 2D model. In addition, we do not know the development of groundwater extraction over time. Based on the available data, we assumed a pumping rate of an equivalent line sink parallel to the coast of 950 m^3/d.

Two stress periods were used for the simulations. The length of the first stress period was 4×10^4 d, this being sufficient to allow the concentration field to reach equilibrium for the assumed natural steady-state situation. The second stress period had a length of 67 years, equivalent to the period between the establishment of Camp McQuaid in 1943 (U.S. Army Corps of Engineers 1997) and the time the TDEM data were collected, in which we apply a uniform pumping rate of 950 m^3/d.

The model was discretized with 500 columns and 25 layers resulting in a cell size of 7 by 1 to 2 m. The transport equation was solved using an implicit finite-difference scheme with upstream weighting. The lengths of transport steps were fixed at 20 d. To investigate the effect of numerical dispersion in our model due to the grid discretization, we compared the simulations of the 25-layer model with a model using 50 layers. These simulations were performed for the parameter values listed in Table 1. The results of the comparison are plotted in Figure 5, showing only a marginal difference between both models. The reduction in the number of layers was important to save computational time associated with the salt water intrusion model and to simplify the generation of the TDEM forward responses. Based on Figure 5, we use 25 model layers for the SEAWAT simulations in this study.

Parameterization

For the CHI-S, we estimate three groups of parameters: parameters pertaining to the salt water intrusion model (γ), the TDEM model (π_u), and parameters associated with the petrophysical relationship described in Equation 1 (p). In Table 3, these parameters are listed together with their starting values and the group they belong to. The parameters for the salt water intrusion model are the following: hydraulic conductivity K_h (m/d), anisotropy K_z/K_h(−), specific yield S_y(−), porosity θ_s(−), longitudinal dispersivity α_L (m), and molecular diffusion D_m (m^2/d).

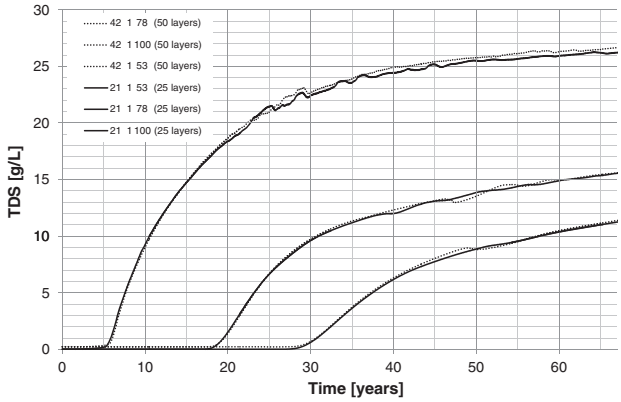

Figure 5. Concentration time series for a model with 50 (dashed) and 25 layers (solid), showing no significant signs of numerical dispersion due to a limited vertical discretization. For the SEAWAT simulations, we will therefore continue to use 25 layers.

The hydraulic conductivity for sand has a large range. Freeze and Cherry (1979), for example, provide a range of 10^3 to 10^5 m/year and Carsell and Parrish (1988) list an average of 29.70 ± 15.60 cm/h. Translated to meters per day, these ranges are 2.7 to 274 m/d and 7.1 ± 3.7 m/d, respectively. Aquifer pump tests by Harding Lawson Associates (1994) at Ford Ord, located 30 km south of the School-site, recorded estimated hydraulic conductivities of ca. 200 to 300 ft/d or 60 to 90 m/d for the Upper 180-foot aquifer, which is hydrostratigraphically similar to the unconfined aquifer at the School-site. As a starting value, we will therefore choose a value of 20 m/d, which is between the average provided by Carsell and Parrish (1988) and the estimates by Harding Lawson Associates. K_z/K_h was set initially to 0.1 and is also an estimable parameter. Its value was chosen to be significantly smaller than 1, due to the presence of layers of fine-grained deposits within the Upper Aromas Sands. Parameters θ_s and S_y are estimated using the following relationship:

$$S_y = \theta_s - \theta_{res} \quad (2)$$

where θ_{res} is the residual water content that is not drainable. We assumed a constant value for this parameter according to Carsell and Parrish (1988), who derived an average value of 0.045 for sandy soils based on 246 samples collected at various sites. For the porosity, we use a starting parameter value of 0.33, which yields a starting parameter value of 0.285 for S_y. The dispersion was separated into longitudinal α_L and transversal dispersivity α_T. α_T was set constant to 10% of the longitudinal dispersivity, which was set initially to a starting value of 10 m. The starting value for molecular diffusion was set to 10^{-4} m^2/d.

Subsurface resistivities were generated from simulated concentrations using the petrophysical relationship described by Equation 1. However, the resistivity of the unsaturated zone and the resistivity of the fresh water-saturated clay layer were not linked to the simulated hydrologic model states. Instead, they were included in π_u or based on the geophysical inversion results in Figure 4A. Table 2 lists in which way the electrical resistivity model is built up to generate a TDEM forward response during the CHI-S.

TDEM-layer 1 represents the unsaturated zone, whose thickness is calculated based on the hydraulic heads simulated in SEAWAT at the TDEM locations. The electrical resistivity of this layer is unknown and will be estimated during the CHI-S. Due to dry cells in the upper 3 to 4 layers in the SEAWAT model, the concentration of layer 5 in the SEAWAT model is used to obtain an electrical resistivity for TDEM-layer 2 by employing the Archie's law. The bottom elevation of TDEM-layer 2 corresponds to the bottom of SEAWAT-layer 5. This was subsequently done for TDEM layers 3 to 22 using the salt concentrations of the SEAWAT model at the sounding locations. The thickness of all these TDEM layers was fixed according to the vertical discretization of the SEAWAT model. TDEM layer 23 was used to take into account the presence of the clay, but its electrical resistivity was not an estimable parameter in the CHI-S. The electrical resistivity and top elevation of layer 23 were based on the prior geophysical inversion results (Figure 4A). We considered these results to provide a proper estimate for the electrical resistivity of the clay as the SEAWAT model does not provide information about this parameter and the inclusion of this parameter in the CHI-S would increase the computational burden.

The cementation factor m, used in the Archie's law to calculate the formation factor together with the porosity (note that the porosity is also an estimable parameter), was fixed to a value of 1.3 representing unconsolidated sands. This value is site-specific, and should be included in the CHI-S whenever possible. Simulations for our study, however, showed a high cross-correlation between the estimated porosity and this Archie's cementation factor, which was fixed for this reason.

Table 2
TDEM-Model Configuration for CHI-S at the School-Site

TDEM Layer	Hydrogeologic Model	Parameter Group
1	Unsaturated zone	π_u
2	Concentration layer 5	
|	|	π_c
22	Concentration layer 25	
23	Clay	Not estimated

The last column shows whether the geophysical parameters are generated from the SEAWAT-model (π_c), separately estimated (π_u), or based on the prior geophysical inversion results.

Table 3
Overview of Estimated Parameters Used in the CHI-S for the School-Site

Parameter	Group	Starting Value	Estimated Value
K_h (m/d)	γ	2.00E+01	2.05E+01 ± 4%
K_z/K_h (−)	γ	0.10	0.12 ± 9%
S_y (−)	γ	0.29	0.39 ± 1%
α_L (m)	γ	1.00E+01	1.30E+01 ± 5%
D_m (m^2/d)	γ	1.00E−04	1.67E−04 ± 8%
θ_s (−)	γ, p	0.33	0.44 ± 1%
Resistivity unsaturated zone (Ωm)	π_u	2.00E+02	2.04E+02 ± 43%
m (−)	Fixed	1.30	
Resistivity clay layer (Ωm)	Fixed	Prior geophysical inversion	

Results

Table 3 shows the parameter estimates resulting from the CHI-S for the TDEM soundings and the SEAWAT model associated with the School-site. Parameters could be resolved fairly well, which is marked by posterior parameter standard deviations of around 10% with respect to the parameter estimates. This was not the case for the estimated electrical resistivity of the unsaturated zone. In the inversion, this parameter was not very sensitive with respect to the geophysical observations. Parameter cross-correlation (Doherty 2010) is shown in Table 4, showing values below 0.8 for all parameters. A number of parameters were close to the starting values listed in Table 3. We tested different starting values for the parameters estimated in the CHI-S, which yielded similar estimates. A common problem of local minima can be faced with gradient-search algorithms such as PEST. Various methods are available to explore parameter space more globally (e.g., Vrugt et al. 2003; Tonkin and Doherty 2009), but at the cost of an additional computational burden due to a more detailed exploration of the objective function surface or the recalibration of additional parameter realizations.

To evaluate the inversion results in Table 3, we now compare the estimated parameter values with the values that are expected based on literature and nearby site investigation reports. Hydraulic conductivity was expected to have slightly higher values, based on the aquifer pump test results by Harding Lawson Associates (1994), but its value is well within the range provided by Freeze and Cherry (1979). Anisotropy was expected to have a value of much <1, but we cannot judge whether 0.12 is low enough. Other studies in this area used anisotropy values of around 0.01 (e.g., Hydrometrics 2009), but these studies are representative for larger scales and the deep aquifer system, where clay layers in the Aromas and Purisma Formation are represented using a higher vertical anisotropy. Porosity and specific yield (which was tied to the porosity through a fixed residual water content) fall within the range provided by Carsell and Parrish (1988). This parameter was one of the most sensitive parameters in this application, which can be explained by the fact that porosity not only controls how far the fresh water/salt water interface moves inland but also affects the conversion of concentrations into electrical resistivities as it is part of the petrophysical relationship. Longitudinal dispersivity was estimated to be around 13 m. Gelhar and Axness (1983) show that dispersivity depends on the scale of a model and indicate 10% of the model scale is a representative estimate for the dispersivity. Using the depth of the aquifer as a representative scale, this value would be 5 m for the School-site model. The estimated dispersivity is also larger than the grid cell sizes, the scale at which scale numerical dispersion acts. Diffusion was estimated around 1.67×10^{-4} m^2/d. This process is often neglected as a contribution to the total dispersive flux (Bond and Bredehoeft 1987). The electrical resistivity of the unsaturated zone should be well above 100 Ωm, which is the case according to Table 3, which shows a value of ca. 200 Ωm.

Figure 6 shows the fit between simulated and measured apparent resistivities for two TDEM soundings. As our model is highly simplified, we do not expect to fit the data perfectly. The right plot in Figure 6 shows the root-mean-square error (RMSE) for each of the TDEM soundings, which should have a value of around 1. For soundings 1 to 3 and sounding 14, the RMSE is significantly larger. The large misfit of soundings 1 to 3 suggests a structural error in either the TDEM model or the salt water intrusion model as the apparent resistivities at the first 6 to 7 time gates are consistently underestimated. This means the electrical resistivity of the upper part of the subsurface is underestimated at these particular sounding locations. Explanations are likely related to the assumption of uniform aquifer properties, a 2D groundwater model, and a uniform electrical resistivity for the unsaturated zone. Furthermore, we used a 1D electrical resistivity model for each sounding, which does not take into account the lateral variations in electrical resistivity that fall within the footprint of the TDEM instrument. For soundings 1 to 3, these lateral variations might be important due to the shape of the salt water/fresh water interface. Another factor that was not taken into account by the 1D TDEM models is the fact that TDEM soundings 1 to 3 were positioned <30 m from the cliffs along the coast line. The presence of these cliffs (which are at a height of $\sim +20$ mamsl) can be important as the resistivity of air is infinitely large. However, based on a number of undocumented TDEM forward responses, the assumption of uniform aquifer properties and the neglecting of

Table 4
Overview of the Parameter Cross-Correlation for the CHI-S

	K_h	K_z/K_h	α_L	D_m	θ_s	Resistivity Unsaturated
K_h	1	−0.76	0.45	0.56	−0.14	0.72
K_z/K_h	−0.76	1	0.78	0.69	0.08	−0.47
α_L	0.45	0.78	1	0.33	0.20	0.52
D_m	0.56	0.69	0.33	1	−0.03	0.07
θ_s	−0.14	0.08	0.20	−0.03	1	−0.48
Resistivity Unsaturated	0.72	−0.47	0.52	0.07	−0.48	1

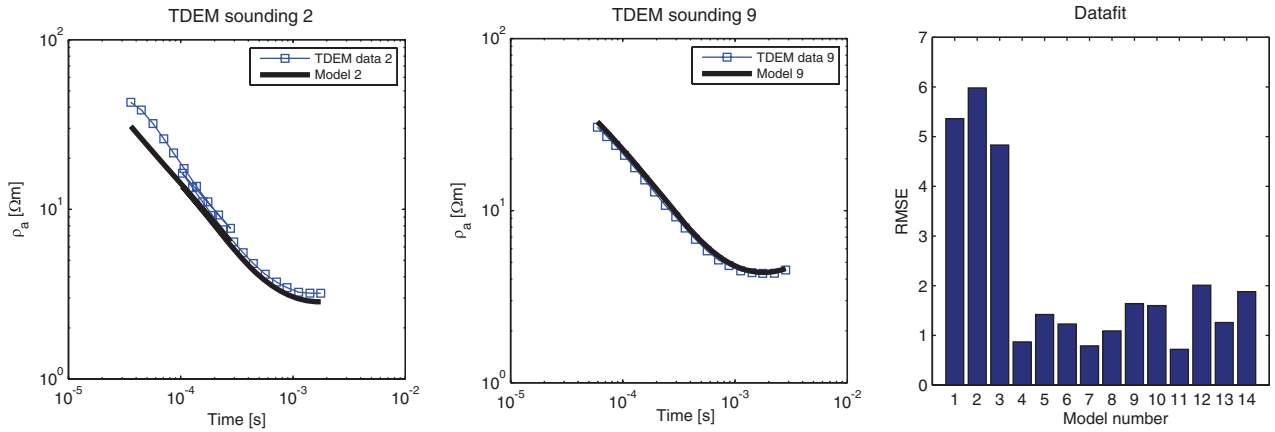

Figure 6. Simulated (solid) and observed (squares) apparent resistivities ρ_a for two TDEM soundings. The right figure indicates the residuals for all 14 TDEM-sounding locations in terms of the RMSE.

3D effects most likely caused the poor data fit for TDEM soundings 1 to 3. The slightly larger RMSE for soundings 12 and 14 can be explained by poor data quality (note TDEM soundings 15 to 19 were not used for this reason).

Figure 4C shows the estimated resistivity model using the CHI-S. The bottom layer in Figure 4C is the same as in Figure 4A as these resistivities were fixed prior to inversion. The top layer in Figure 4C represents the unsaturated zone, which had an estimated electrical resistivity of 196 Ωm. In contrast to Figure 4A and 4B, Figure 4C includes the distinction between the saturated and unsaturated zone, as the bottom elevation of the top resistivity layer is equal to the simulated water table by the SEAWAT-model. The second difference with respect to Figure 4A and 4B is the increased amount of detail for the electrical resistivity distribution in the unconfined aquifer. Furthermore, the electrical resistivity model resulting from the 25-layer smooth inversion shows a much less consistent pattern about the distribution of salt and fresh water in the aquifer. Of course, this can be not only due to spatial heterogeneity, but also due to the definition of the smoothness constraints in the geophysical model that do not provide information about the mechanism behind salt water intrusion. Given the simple salt water intrusion model, the data fit, and the small number of parameters that could be resolved well (Table 3), the salt water intrusion model provided a well-defined regularization framework for inverting the TDEM data.

In Figure 7, we plot the result of the SEAWAT simulations for the calibrated model, representing the salt concentration distribution of the unconfined aquifer after 67 years of pumping at the School-site. The black line in Figure 7 marks the simulated 10% sea water line for 1943, before pumping commenced.

Discussion and Conclusions

In this study, we investigated the application of the CHI approach to estimate the hydraulic properties of a salt water intrusion model with TDEM data. In this CHI approach, to which we refer as the CHI-S, simulated hydrologic state variables are translated to a geophysical model. In short, a hydrological model is used to interpret the geophysical data. We modified the existing CHI-S frameworks of Kowalsky et al. (2005), Lambot et al. (2009), Hinnell et al. (2010), and Pollock and Cirpka (2010) as these methods do not include the direct estimation of geophysical model parameters that cannot be computed from a set of hydrologic simulations. However, these parameters might be essential to fit the geophysical data satisfactory.

We employed our CHI-S approach for a field site in Santa Cruz County, California. In this region, salt water intrusion has been occurring (Hanson 2003) as a result of groundwater extraction. For this site, we collected a TDEM dataset and developed a cross-sectional salt water intrusion model in SEAWAT, representing the unconfined aquifer system at this location. Based on a separate geophysical inversion of the TDEM data, we could detect a confining geological unit, marking the hydrologic base of the unconfined aquifer. With the CHI-S, we could successfully estimate parameter values for the main hydraulic properties of the aquifer, using the data of 14 TDEM soundings that comprised more than 300 apparent resistivities.

The electrical resistivity models that resulted from the CHI-S provided a significant improvement in spatial resolution, which would be very difficult to obtain with a traditional geophysical inversion approach as the complex spatial correlation between the inverted geophysical parameters cannot be captured with standard regularization constraints. Furthermore, the discretization of the electrical resistivity model in the CHI-S was consistent with that of the salt water intrusion model and incorporated a division between unsaturated and water-saturated sediments.

In the SHI, electrical resistivity models would be used that result from a traditional geophysical inversion technique, leading to errors associated with the regularization constraints, inconsistency in scales, and the neglecting of distinct hydrogeological features and mechanisms.

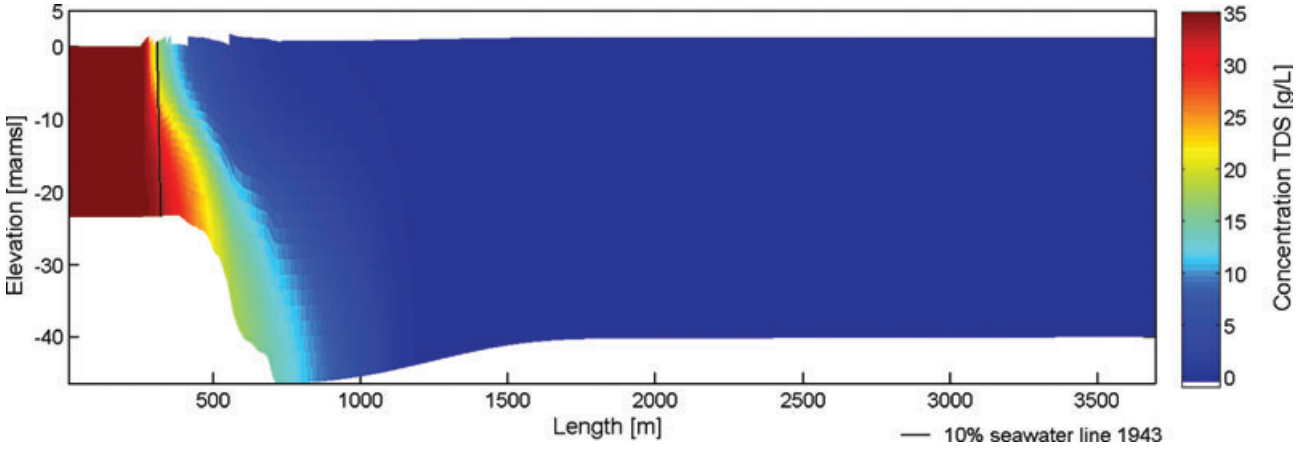

Figure 7. Concentration distribution after 67 years of pumping (950 m^3/d) at the School-site for the SEAWAT model calibrated with the TDEM data using a CHI-S. The black line indicates the simulated steady-state position of the 10% sea water line in 1943.

As shown, these problems can be overcome by applying the CHI-S. Traditional geophysical inversion methods are still essential, though, in order to assess the sensitivity of the TDEM data to the salt water-saturated sediments and the hydrogeological structure of a region or site.

For most TDEM soundings at the field site, the level of data fit was acceptable; however, a structural underestimation of apparent resistivities was found for the early time gates pertaining to three soundings located closest to the ocean. Possible explanations for this underestimation can be attributed to the specific setup of the salt water intrusion model, the lack of hydrogeologic data, and the simulated TDEM data. The simplifications in the salt water intrusion model comprised, for example, the assumption of uniform aquifer properties, the use of a cross-sectional model for a 3D groundwater problem, and the estimated values for pumping rates and recharge. For the generation of the TDEM forward responses, we assumed a 1D-layered earth model, which neglects lateral variations in electrical resistivity due to the presence of topography (e.g., cliffs) and the shape of the fresh water/salt water interface. Furthermore, the TDEM-sounding locations were not perfectly aligned with the main groundwater flow direction and no water level and concentration measurements were available to be used in the CHI-S.

Despite the previous-mentioned limitations, we have shown that a salt water intrusion model can offer an excellent interpretation framework for TDEM data collected in coastal areas. This could not only be important to improve the simulation of the past system state of a coastal aquifer with salt water intrusion models, but also provides an opportunity to use TDEM data and salt water intrusion models consistently as a real-time monitoring tool to support current groundwater management. The CHI-S approach we developed in this study could be simultaneously used with the CHI-P approach that was developed in Herckenrath et al. (unpublished data), in which geophysical parameters (P) are coupled with hydrologic model parameters (e.g., hydraulic conductivities) instead of the simulated hydrologic state variables. Both the CHI-S and CHI-P could offer a flexible tool to fully exploit the hydrogeologic information contained within geophysical measurement data.

Acknowledgments

This work was supported by the Danish Agency for Science Technology and Innovation funded project RiskPoint-Assessing the risks posed by point source contamination to groundwater and surface water resources under grant number 09-063216. The costs of the fieldwork at Monterey Bay were covered by funding from the S. D. Bechtel, Jr. Foundation to R. Knight and P. Kitanidis, Stanford University. The authors would like to thank Jay Ketelsen and the Monterey Bay Academy for providing access to the field site.

References

Abdalla, O.A.E., M. Ali, K. Al-Higgi, H. Al-Zidi, I. El-Hussain, and S. Al-Hinai. 2010. Rate of seawater intrusion estimated by geophysical methods in an arid area: Al Khabourah, Oman. *Hydrogeology Journal* 18: 1437–1445.

Adepelumi, A.A., B.D. Ako, T.R. Ajayi, O. Afolabi, and E.J. Omotoso. 2009. Delineation of saltwater intrusion into the freshwater aquifer of Lekki Peninsula, Lagos, Nigeria. *Environmental Geology* 56: 927–933.

Archie, G.E. 1942. The electrical resistivity log as an aid in determining some reservoir characteristics. *Transactions of the American Institute of Mining and Metallurgical Engineers* 146: 54–61.

Auken, E., A.V. Christiansen, L.H. Jacobsen, and K.I. Sorensen. 2008. A resolution study of buried valleys using laterally constrained inversion of TEM data. *Journal of Applied Geophysics* 65, no. 1: 10–20.

Auken, E., L. Pellerin, A.V. Christiansen, and K. Sorensen. 2006. A survey of current trends in near-surface electrical and electro-magnetic methods. *Geophysics* 71, no. 5: G249–G260.

Bauer-Gottwein, P., B.N. Gondwe, L. Christiansen, D. Herckenrath, L. Kgotlhang, and S. Zimmermann. 2009. Hydrogeophysical exploration of three-dimensional salinity

anomalies with the the time-domain electromagnetic method (TDEM). *Journal of Hydrology* 380, no. 3–4: 318–329.

Bond, L.D., and J.D. Bredehoeft. 1987. Origins of seawater intrusion in a coastal aquifer—A case-study of the Pajaro Valley, California. *Journal of Hydrology* 92, no. 3–4: 363–388.

Carsell, R.F., and R.S. Parrish. 1988. Developing joint probability distributions of soil water retention characteristics. *Water Resources Research* 24, no. 5.

CH2M/Hill. 2005. *Hydrogeologic Assessment of the Seaside Groundwater Basin: Report Prepared for Somach.* Simmons & Dunn and California: American Water Co.

Commer, M., and G. Newman. 2004. A parallel finite-difference approach for 3D transient electromagnetic modeling with galvanic sources. *Geophysics* 69, no. 5: 1192–1202.

Doherty, J. 2010. *PEST: Model-Independent Parameter Estimation.* Brisbane, Queensland, Australia: Watermark Numerical Computing. http:/www.pesthomepage.org (accessed March 9, 2012).

Duque, C., M.L. Calvache, A. Pedrera, W. Martin-Rosales, and M. Lopez-Chicano. 2008. Combined time domain electromagnetic soundings and gravimetry to determine marine intrusion in a detrital coastal aquifer (Southern Spain). *Journal of Hydrology* 349, no. 3–4: 536–547.

Effersø, F., E. Auken, and K.I. Sorensen. 1999. Inversion of band-limited TEM responses. *Geophysical Prospecting* 47, no. 4: 551–564.

Farquharson, C.G., and D.W. Oldenburg. 1993. Inversion of time-domain electromagnetic data for a layered Earth. *Geophysical Journal International* 114: 433–442.

Ferré, T., L. Bentley, A. Binley, N. Linde, A. Kemna, K. Singha, K. Holliger, J.A. Huisman, and B. Minsley. 2009. Critical steps for the continuing advancement of hydrogeophysics. *Eos, Transactions, American Geophysical Union* 90, no. 23: 200–201.

Fitterman, D.V., and W.L. Anderson. 1987. Effect of transmitter turn-off time on transient soundings. *Geoexploration* 24, no. 2: 131–146.

Fitterman, D.V., and M.T. Stewart. 1986. Transient electromagnetic sounding for groundwater. *Geophysics* 51, no. 4: 995–1005.

Freeze, A.R., and J.A. Cherry. 1979. *Groundwater.* Englewood Cliffs, New Jersey: Prentice Hall Inc.

Frohlich, R.K., D.W. Urish, J. Fuller, and M. O'Reilly. 1994. Use of geoelectrical methods in groundwater pollution surveys in a coastal environment. *Journal of Applied Geophysics* 32: 139–154.

Gelhar, L.W., and C.L. Axness. 1983. 3-Dimensional stochastic-analysis of macrodispersion in aquifers. *Water Resources Research* 19, no. 1.

Giambastiani, B.M., M. Antonellini, G.H. Essink, and R.J. Stuurman. 2007. Saltwater intrusion in the unconfined coastal aquifer of Ravenna (Italy): A numerical model. *Journal of Hydrology* 340, no. 1–2: 91–104.

Goldman, M., D. Gilad, A. Ronen, and A. Melloul. 1991. Mapping of seawater intrusion into the coastal aquifer of israel by the time domain electromagnetic method. *Geoexploration* 28, no. 2: 153–174.

Hanson, T.H. 2003. *Geohydrologic Framework of Recharge and Seawater Intrusion in the Pajaro Valley, Santa Cruz and Monterey Counties*, California: U.S. Geological Survey, Water-Resources Investigations Report 03–4096.

Harding Lawson Associates. 1994. *Basewide Remedial Investigation/Feasibility Study.* Fort Ord, California: Harding Lawson Associates, Appendix E: Aquifer test results.

HGG. 2011. *Getting Started With SiTEM and Semdi.* Denmark: Department of Earth Sciences, University of Aarhus. http://geofysiksamarbejdet.au.dk (accessed February 27, 2012).

Hinnell, A., T. Ferre, J. Vrugt, J. Huisman, S. Moysey, J. Rings, and M. Kowalsky. 2010. Improved extraction of hydrologic information from geophysical data through coupled hydrogeophysical inversion. *Water Resources Research* 46.

Hydrometrics, L.L.C. 2009. Seaside groundwater basin modeling and protective groundwater elevations. Report prepared for Seaside Basin Watermaster. Oakland, California.

Kirsch, R. 2006. *Petrophysical Properties of Permeable and Low-Permeable Rocks, Groundwater Geophysics.* Berlin Heidelberg: Springer. ISBN: 978-3-540-29387-3.

Koukadaki, M.A., G.P. Karatzas, M.P. Papadopoulou, and A. Vafidis, 2007. Identification of the saline zone in a coastal aquifer using electrical tomography data and simulation. *Water Resources Management* 21: 1881–1898.

Kowalsky, M.B., S. Finsterle, J. Peterson, S. Hubbard, Y. Rubin, E. Majer, A. Ward, and G. Gee. 2005. Estimation of field-scale soil hydraulic and dielectric parameters through joint inversion of GPR and hydrological data. *Water Resources Research* 41, no. 11.

Lambot, S., E. Slob, J. Rhebergen, O. Lopera, K.Z. Jadoon, and H. Vereecken. 2009. Remote estimation of the hydraulic properties of a sand using full-waveform integrated hydrogeophysical inversion of time-lapse, off-ground GPR data. *Vadose Zone Journal* 8, no. 3: 743–754.

Langevin, C.D., and W.X. Guo. 2006. MODFLOW/MT3DMS-based simulation of variable-density ground water flow and transport. *Ground Water* 44, no. 3: 339–351.

Langevin, C.D., D. Fitterman, and M. Deszcz-Pan. 2003. Calibration of a variable-density groundwater flow model using detailed airborne geophysical data. In *Proceedings Second International Conference on Saltwater Intrusion and Coastal Aquifers—Monitoring, Modeling and Management*, Merida, Mexico.

Lebbe, L., N. Van Meir, and P. Viaene. 2008. Potential implications of sea-level rise for Belgium. *Journal of Coastal Research* 24, no. 2: 358–366.

Lesmes, D.P., and S.P. Friedman. 2005. Relationships between the electrical and hydrogeological properties of rocks and soils. *Water Science and Technology Library* 50, Part 2: 87–128.

Macaulay, S., and I. Mullen. 2007. Predicting salinity impacts of land-use change: Groundwater modelling with airborne electromagnetics and field data, SE Queensland, Australia. *International Journal of Applied Earth Observation and Geoinformation* 9, no. 2: 124–129.

Mann, J.F. 1988. Regarding Overdraft and Seawater Intrusion: Letter to General Manager of Pajaro Valley Water Management Agency, January, 8 pp. Monterey, California.

Mullen, I., K. Wilkinson, R. Cresswell, and J. Kellett. 2007. Three-dimensional mapping of salt stores in the Murra-Darling Basin, Australia—2. Calculating landscape salt loads from airborne electromagnetic and laboratory data. *International Journal of Applied Earth Observation and Geoinformation* 9, no. 2: 103–115.

Newman, G.A., G.W. Hohmann, and W.L. Anderson. 1986. Transient electromagnetic response of a 3-dimensional body in a layered earth. *Geophysics* 51, no. 8: 1608–1627.

Oldenburg, D.W. 1990. Inversion of electromagnetic data: An overview of new techniques. *Surveys in Geophysics* 11: 231–270.

Pollock, D., and O.A. Cirpka. 2010. Fully coupled hydrogeophysical inversion of synthetic salt tracer experiments. *Water Resources Research* 46.

Supper, R., K. Motschka, A. Ahl, P. Bauer-Gottwein, B. Gondwe, G.M. Alonso, A. Roemer, D. Ottowitz, and W. Kinzelbach. 2009. Spatial mapping of submerged cave systems by means of airborne electromagnetics: An emerging technology to support protection of endangered karst aquifers. *Near Surface Geophysics* 7, no. 5–6: 613–627.

Tonkin, M., and J. Doherty. 2009. Calibration-constrained Monte Carlo analysis of highly parameterized models using subspace techniques. *Water Resources Research* 45.

Topp, G.C., J.L. Davis, and A.P. Annan. 1980. Electromagnetic determination of soil-water content—Measurements in coaxial transmission-lines. *Water Resources Research* 16, no. 3: 574–582.

U.S. Army Corps of Engineers. 1997. *Preliminary Assessment Camp McQuaide*. Santa Cruz County, California: U.S. Army Corps of Engineers.

Vrugt, J.A., H.V. Gupta, W. Bouten, and S. Sorooshian. 2003. A shuffled complex evolution Metropolis algorithm for optimization and uncertainty assessment of hydrologic model parameters. *Water Resources Research* 39, no. 8.

Wang, T., and G.W. Hohmann. 1993. A finite-difference, time-domain solution for 3-dimensional electromagnetic modeling. *Geophysics* 58, no. 6: 797–809.

Ward, S.H., and G.W. Hohmann. 1988. Electromagnetic theory for geophysical applications. In *Electromagnetic Methods in Applied Geophysics*, ed. M.N. Nabighian, 131–311. New York: Society of Exploration Geophysicists (SEG).

Zhang, Q., R.E. Volker, and D.A. Lockington. 2004. Numerical investigation of seawater intrusion at Gooburrum, Bundaberg, Queensland, Australia. *Hydrogeology Journal* 12, no. 6: 674–687.